A new global model to characterise the dynamics of a pneumatic proportional-pressure valve for a biomechatronic application

Silvia E. Rodrigo, Claudia N. Lescano & Héctor D. Patiño

Journal of the Brazilian Society of Mechanical Sciences and Engineering

ISSN 1678-5878

J Braz. Soc. Mech. Sci. Eng.
DOI 10.1007/s40430-016-0591-x

Springer

J Braz. Soc. Mech. Sci. Eng.
DOI 10.1007/s40430-016-0591-x

TECHNICAL PAPER

A new global model to characterise the dynamics of a pneumatic proportional-pressure valve for a biomechatronic application

Silvia E. Rodrigo[1] · Claudia N. Lescano[1,2] · Héctor D. Patiño[3]

Received: 4 January 2016 / Accepted: 22 June 2016

Abstract Traditionally, the pneumatic proportional-pressure valve dynamics has been characterised from its output pressure and input reference voltage relationship. However, in our application about the use of a pneumatic artificial muscle as actuator of a gait rehabilitation exoskeleton, where an adequate valve output pressure control is required to simultaneously attain a smooth joint movement and an efficient interaction force with the patient, it is also important to evaluate the effect on valve output pressure of the input airflow rate disturbance caused by downstream load variations during this actuator operation. In this paper we present a new global linear model for such application, considering the concurrent effect on valve output of both voltage and airflow rate inputs. From data acquired through an experimental setup and for reference inputs in the frequency range of human gait, two transfer functions describing the relationships between valve output pressure and their respective inputs were first obtained. Second, the individual models were combined in a global one, according to the superposition principle. Third, the resultant model was analysed in the time and frequency domains and finally, validated (MSE = 0.0499) and discussed, in the search for clues to design a suitable actuation system for this type of robotic device.

Keywords Pneumatic valve · Dynamic model · Actuation system · Gait rehabilitation

1 Introduction

The expression gait rehabilitation exoskeleton refers to an external structural mechanism that interacts in parallel with the considered patient, transferring mechanical power through joint actuators to actively assist the movement of his/her lower limbs during gait training in a treadmill, combined with partial body weight support [1–3]. Such is the case of our planned biomechatronic application, related to the design of an active ankle–foot orthosis (AAFO). The final purpose is to compensate during gait training and through an adequate actuation system of the AAFO, the dysfunction of such joint caused by the paralysis of the ankle plantar-flexor muscle group, which typically exhibits patients with incomplete spinal cord injury at lumbosacral level (iSCI) [4].

It is well established that in normal gait conditions, this muscle group is the main source of active power for forward propulsion of the human body in the sagittal plane [5], principally for about 60 % of the gait cycle, where the ankle plantar-flexor muscles, controlled through signals from the central nervous system, generate the most active contraction force (around three to four times the body weight) so as to ensure forefoot takeoff and propel the lower limb from gait stance to swing phase [6]. It is also known that to counteract the effects of applied external loads and disturbances throughout gait cycle, the ankle joint varies its mechanical stiffness (the inverse of compliance), by means

Technical Editor: Sadek C. Absi Alfaro.

✉ Silvia E. Rodrigo
srodrigo@gateme.unsj.edu.ar

[1] Medical Technology Cabinet, National University of San Juan, San Juan, Argentina

[2] National Council of Scientific and Technical Research, Buenos Aires, Argentina

[3] Automatic Institute, National University of San Juan, San Juan, Argentina

Published online: 28 June 2016

of a change of both the articular movement and the force exerted by the muscles attached to it [7].

Among the different class of joint actuators used in such robotic devices to emulate this complex muscle function during gait [8–11], the pneumatic artificial muscle (PAM) emerges as one of the best due to its mechanical behaviour similar to human skeletal muscle [11, 12]. Some of these properties are its high power-to-weight ratio that significantly reduces power consumption and its variable inherent compliance, which allows an optimal adaptation and interaction with the human operator [13, 14]. In contrast, due to its non-linear dynamics [14–16], it is difficult to accurately control the PAM operation so as to achieve simultaneously, a smooth joint movement and a precise regulation of the force exerted by it as part of an AAFO for gait rehabilitation in iSCI patients.

In this sense, a common practice to regulate the pressure within the PAM is through a pair of high-speed on–off valves, commanded by pulsewidth modulation for switching the valve openings at a maximum operating frequency of 350 Hz [17]. Although the pulsewidth modulation setup is easy to interface, it has the drawbacks of requiring a controller to commands the valve and producing electromagnetic noise that affect the functioning of other circuits.

An alternative to solve such drawbacks is using a proportional-pressure regulator valve (PPRV), characterised by the fine-grained control of its output port and the less noisy operation than a pulsewidth modulation setup [17]. In this valve type, the input variable is continuously compared with the output pressure, so that if a system deviation occurs, the PPRV tends to adjust its output accordingly. Besides, the previous works about industrial applications report a 5 Hz bandwidth for this type of pressure valve [18], which is within the typical frequency range of human gait, both in normal (minimal between 0.25 and 0.4, maximal 1.5 Hz) [19] and iSCI subjects (0.125–1.25 Hz) [20].

However, prior to define whether a PPRV-PAM system within an AAFO satisfies the requirements of our planned application, it is central to precisely identify the PPRV dynamic performance. The identification of such performance implies characterising the valve dynamics both in terms of their reference voltage and airflow rate inputs in the time and frequency domains. With such purpose, different parametric [21] and non-parametric [22] methods have been used to develop linear and non-linear dynamic models of the pneumatic pressure valves for industrial applications.

As an example, using parametric methods and based on the main internal mechatronic devices of a PPRV, a valve dynamic global model was formulated [18, 23, 24] and validated in the time and frequency domains [18, 25] by comparing the experimental and simulated responses for several voltage inputs and set downstream loads. In addition, a detailed procedure has been described to attain pneumatic servo-valves models from experimental input and output data, which provide information about its dynamics without considering its mechatronic design [26–28].

Though these previous research works offer the best general approach for modelling any PPRV featuring a similar mechatronic design and internal structure, the state of the art does not show a PPRV model, whose dynamic response has been simultaneously modelled and validated in terms of its both referred inputs for a biomechatronic application, such as those here proposed. This latter issue is considered key when a pressure valve must supply airflow to a variable downstream load, which in this case is represented by the PAM operation [13, 14].

Based on this background, the aim of this comprehensive work was to identify, model, and validate the dynamics of the commercial PPRV-type Festo® VPPM 6L-L-1-G18-0L10H-V1 [29] that will be used to control the PAM operation as part of an AAFO for gait rehabilitation. To fulfil this aim, the following procedure was applied. Section 2 reviews the manufacturer's technical specifications of the analysed valve. Section 3 details the experimental setup used to calibrate the measurement instruments and identify the PPRV static and dynamic behaviours by means of input and output data.

Besides, Sect. 4 describes the methodology used to estimate the valve outlet and inlet airflow rates from the ideal gases state and continuity equations. Section 5 presents the individual linear models achieved to characterise the relationships between the valve output pressure and their both reference voltage and airflow rate inputs, and from them, the valve global model attained in accord with the superposition principle. Section 6 shows the results of the models analysis and validations in the time and frequency domains. Finally, under the framework of our planned biomechatronic application, Sect. 7 exposes the discussion and conclusions of this work, in the search for clues to design a suitable actuation scheme based on a PPRV-PAM system for this class of robotic device.

2 Characteristic of the pneumatic pressure valve

A review of functional features specified by the manufacturer indicates that the PPRV-type Festo® VPPM 6L-L-1-G18-0L10H-V1 is a 3/2-way valve, normally closed (pressure regulation range 0.02–10 bars; standard accuracy 2 %; pressure maximal hysteresis 50 mbar), which offers infinite adjustment of pressure and, thus, of the force or torque, enabling the user to pre-set pressures electrically through a reference voltage between 0 and 10 Vdc [29]. Reliable pressure regulation with multi-sensor control is viable by selecting into three operation modes: fast, universal, and precise. Figure 1 shows a block diagram of the PPRV structure, with its closed-loop control (CLC) circuit.

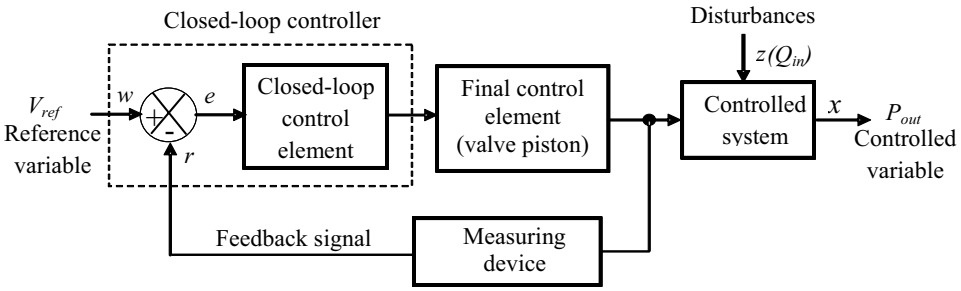

Fig. 1 Block diagram of the mechatronic structure for the analysed PPRV

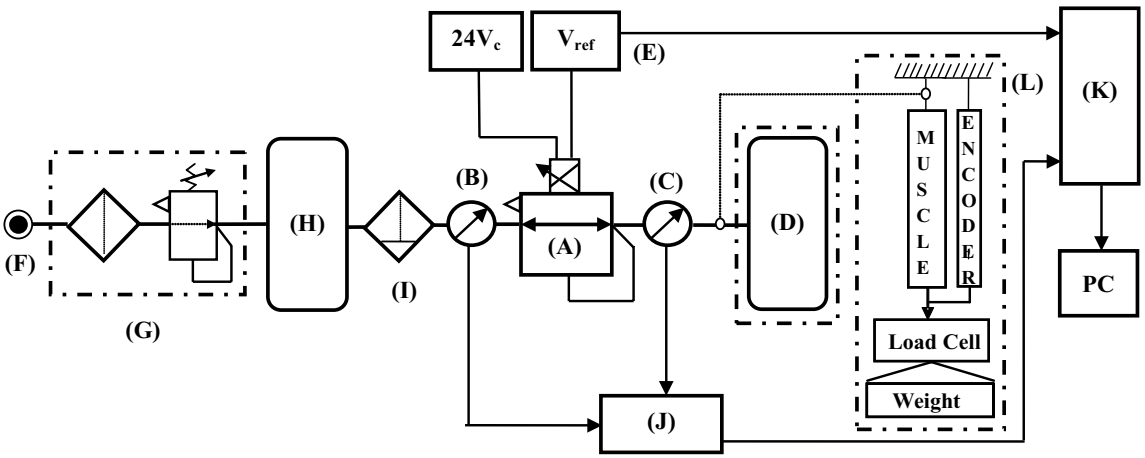

Fig. 2 Experimental test bench setup implemented for PPRV analysis

According to Fig. 1, the reference variable w at the CLC circuit initially acts on a comparator along with the feedback signal r, resulting from the measurement of controlled variable x. Then, the CLC circuit senses the system deviation e and drives the final control element, acting its output directly on the controlled system to compensate the difference between the reference w and the controlled x variables. This process runs continuously so changes in w are always detected.

Though a system deviation will also appear if the reference variable w is constant, but the controlled variable x changes, such as in the case of an airflow rate fluctuation through the valve due to a switching action, a cylinder movement or a load variation. Thus, the disturbance variable z (named Q_{in} for our application) will cause a system deviation, e.g., through a pressure drop in the air supply. As in the previous case, the disturbance variable z will act on the controlled variable x, showing the ability of the regulator to readjust the controlled variable x to the reference variable w.

Such behaviour is described at the manufacturer's datasheets through the valve output pressure versus airflow rate curves with a major or minor slope in the function of the accuracy stated. Here, the analysed PPRV, according to its datasheets [29], keeps a constant value of its output pressure for an airflow rate of up to 100 times its value, a matter that will be evaluated in the following sections.

3 Experimental setup

To identify the dynamics of the evaluated PPRV, several experimental tests were achieved. In Fig. 2, a schematic view of the employed test bench is shown, including the components: valve (A); pressure cells to measure valve inlet and outlet pressures (B and C); 0.04 m^3 volume tank for charge and discharge (D); power supply (E) for PPRV reference voltage; pneumatic circuit (F-G-H-I); signal conditioning circuit (J); data acquisition board (K); and pneumatic artificial muscle along with its measurement elements (L). In addition, 24 Vdc and 12 Vdc from fixed power supply were applied to the PPRV and pressure cells, respectively. Such components are described in detail below.

– *Proportional Pressure Regulator Valve (A)* the universal mode, commonly used in several applications, was selected for its operation [29]. Two types of reference signals were supplied to PPRV by a signal generator (E) so as to map the valve work space: step volt-

ages and 0.4–2 Hz periodic signals, in accord with the human gait frequency range [19, 20].

- *Pneumatic circuit* a compressor (F) with 30 kg/cm^2 capacity provides compressed air that is stored in a reservoir tank (H) to stabilize and supply a constant upstream pressure to the valve regulated through a pressure filter-regulator unit (G). The supply absolute pressure was set at 7 bar, considering the PAM operating conditions in terms of the required force for our application [6, 15]. The air flows through the accumulator tank H and then across a water trap filter (I) and the PPRV, which regulates the pressure inside the downstream tank (D) based on a reference voltage (E).
- *Valve inlet pressure transducer (B)*: MBS 1700 Danfoss® model measures and verifies whether the PPRV inlet pressure corresponds to the gauge pressure value supplied by the compressor.
- *Valve outlet pressure transducer (C)*: AKS 330 Danfoss® model measures the gauge pressure supplied by the PPRV to the downstream connected tank or PAM.
- *Signal conditioning board (J)*: to record the pressure signals, the output signal (4–20 mA) from the upstream and downstream pressure cells was converted in a voltage on a 500 Ω resistor.
- *Data acquisition board (K)*: The NI USB-6009 National Instrument® model was used due to its sampling rate, data communication by USB port, and software versatility. Signals from pressure cells and PPRV reference voltage were acquired through their analogic inputs, employing a Labview® Virtual Instrument for data capture and storage. The signals from measuring instruments were also digitalised and later sent to a PC for processing and visualization of results.

Besides, for the probes with the PPRV-PAM system, the tank (D) was replaced by the (L) system, composed by a PAM and its measuring elements. The PAM model is the DMSP-40-400 N-RM-CM Festo®, 400 mm nominal length and 40 mm inside diameter, capable of exerting a maximum force of 6000 N for a 1–6 bar range of operating pressures, and developing a maximal permissible contraction of 25 % of its nominal length [30]. As well, the PAM longitudinal displacement and the force exerted by it were, respectively, measured by a linear encoder and a load cell.

In addition, the referred experimental setup was used for static calibration of the measurement instruments and the valve. In the first case, it was achieved for a supply absolute pressure of 7 bars and constant values of voltage inputs (0–5 Vdc range) applied to the valve. For the PPRV static calibration, different voltage values at 1 V steps as reference signals were applied and the valve output pressure in vacuum (without downstream load) was measured by a Fluke® Serie 700 P27 pressure module, 0–20 bar range, associated with a Fluke® 725 multifunction process calibrator. Figure 3 shows the results of PPRV static calibration in terms of outlet relative pressure versus inlet reference voltage.

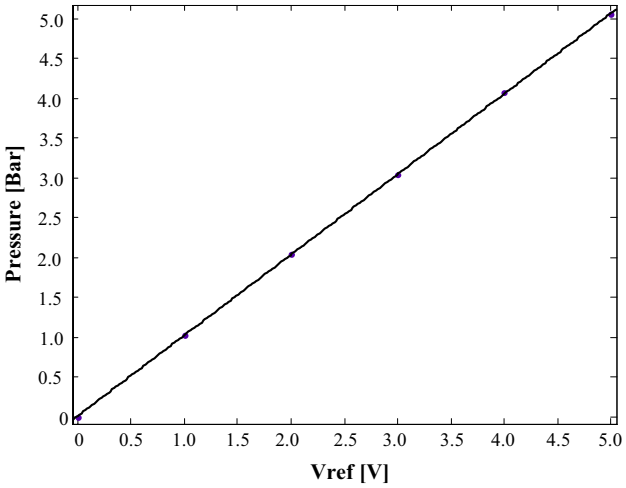

Fig. 3 Static calibration curve for the PPRV at 7 bars supply absolute pressure

4 Modelling airflow through the valve

To identify the PPRV performance across the range of airflow rates associated with the valve working space in general and particularly, with the PAM operation, the valve input and output pressures and flow rates were determined through several tests carried out from the mentioned experimental setup. In agreement with the standard ISO 6358 [31], the airflow rate through the type of here analysed valve is expressed as:

$$q_{out} = Cp_{in}\sqrt{\frac{T_{in}}{T_{out}}}\sqrt{1-\left(\frac{\frac{p_{out}}{p_{in}}-b}{1-b}\right)^2} \quad for\ \frac{p_{out}}{p_{in}} \rangle b \quad \text{subsonic flow} \tag{1}$$

$$q_{out} = Cp_1\sqrt{\frac{T_{in}}{T_{out}}} \quad for\ \frac{p_{out}}{p_{in}} \leq b \quad \text{chocked flow} \tag{2}$$

where q_{out} is the volumetric flow rate (m^3/s); p_{in} and p_{out} are the valve inlet and outlet pressures (bars), respectively; b is the critical pressure ratio; C is the sonic conductance (m^3/s bar); and T_{in} and T_{out} are the inlet and outlet temperatures = 298°K, respectively.

These equations were used to estimate the values of C and b, which provide a mapping of the valve working space. To reduce the complexity of this model, it was

assumed that all connecting tubes are very short and there are not sharp angle connectors, as this would increase pressure losses. Details of the applied procedure for calculation of C and b and its results, both for charge and discharge of a 0.04 m^3 volume tank connected downstream to the valve, are shown in the Appendix of this work.

As regard the calculation of airflow rate through the valve for the PPRV-PAM system, although the standard ISO 6358 specifies the measurement setup suitable to estimate the dependence of C and b with respect to the valve diaphragm aperture degree, this standard model provides a poor adjustment for containers of small volumetric capacity, such as in the case of the here considered PAM. Thus, a different procedure based on the ideal gases state and the continuity equations was utilized for estimating the valve inlet and outlet flow rates [17] for such system.

In this downstream load situation assessed at isothermal conditions during PAM operation, the airflow rate through PPRV depends not only on the pressure variations described by the standard ISO 6358 [30], but also on the PAM volume change over time. In effect, due to this PAM volume variation, the flow rate through the valve, equal to the flow rate through PAM (q_{PAM}), is given by:

$$q_{\mathrm{PAM}} = \frac{V_{\mathrm{PAM}}}{\kappa RT}\dot{p}_{\mathrm{out}} + \frac{1}{\kappa RT}\frac{\mathrm{d}V_{\mathrm{PAM}}}{\mathrm{d}x}\dot{x}p_{\mathrm{out}} \tag{3}$$

where $\dot{p}_{\mathrm{out}}$ is the valve output pressure derivative (bar/s); V_{PAM} is the PAM volume (m^3); x is the PAM contraction (= actual length-nominal length/nominal length); $\dot{x}$ is the PAM contraction derivative; κ is the conversion factor; R is the gas ideal constant = 286,9 J/Kg°K; and T is the temperature = 298°K.

In addition, considering the muscle volume dependence on its length variation, it can be estimated using geometric parameters of the muscle. In this case, the PAM was modelled as a cylinder of variable volume in the function of the contraction changes experimented during its operation, which can be approximated by a third-order polynomial [16], according to:

$$V_{\mathrm{PAM}}(x) = ax^3 + bx^2 + cx + d \tag{4}$$

where a, b, and c are the polynomial coefficients obtained from the Curve Fitting Toolbox of Matlab®. Then, combining (3) and (4), the valve outlet flow rate for the variable downstream load due to PAM operation was estimated and the contribution that the pressure and volume variations made on it was evaluated. Regarding to the valve inlet flow rate, it was calculated from the corresponding value of valve outlet flow rate in agreement with the continuity equation [17].

During the experimental tests, the valve supply absolute pressure was set at 7 bar, and two reference voltage conditions at a frequency of 1.5 Hz was evaluated: ranges of 0–3 V and 0–5 V with duty cycle of 50 %. Besides the valve inlet and outlet pressures, the PAM longitudinal displacement and the force exerted by PAM were dynamically registered through their respective measurement elements. In addition, a series of weights in the range of 250–3000 N were downstream connected to PAM [15], which exerts a pulling force on it. In particular, in this work, a weight of 893 N, simulating the body mass of 91.3 kg of an adult subject wearing the AAFO was assessed. Finally, a comparison between the valve inlet and outlet flow rates for the PPRV-PAM system was made to determine if there exists significant difference between both airflow rates.

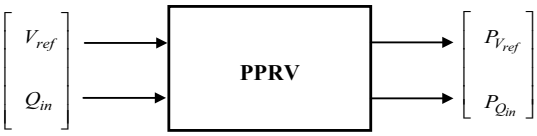

Fig. 4 Schematic diagram of the linear system represented for the PAM operation

5 Identification of PPRV global dynamic behaviour

The control system theory establishes that a system is linear whether it fulfils the superposition principle [32]. Specifically applying this principle to the here analysed PPRV (where, from Fig. 1, its inputs are symbolized by the reference voltage V_{ref} and the airflow rate Q_{in} variables, and its output by the valve output pressure, P_{out}), it states that if a system has more than one input variable, the total or overall output will be equal to the sum of the partial outputs $P_{V_{\mathrm{ref}}}$ and $P_{Q_{in}}$, which result from evaluating each input separately, while the other entry remains null (Fig. 4), in agreement with:

$$\begin{aligned} P_{\mathrm{out}} &= P_{V_{\mathrm{ref}}} + P_{Q_{\mathrm{in}}} \\ P_{\mathrm{out}} &= G_{V_{\mathrm{ref}}}\big|_{Q_{\mathrm{in}}=0} * V_{\mathrm{ref}} + G_{Q_{\mathrm{in}}}\big|_{V_{\mathrm{ref}}=0} * Q_{\mathrm{in}} \end{aligned} \tag{5}$$

where $G_{V_{\mathrm{ref}}}$ and $G_{Q_{\mathrm{in}}}$ indicate the transfer functions corresponding to each respective input.

However, strictly speaking, most real physical systems, including the pneumatic valves, are in some degree nonlinear, so the concept of linearity of a system is an abstraction made to reduce the complexity of its dynamics analysis. In this sense, the feedback control systems are ideal models constructed to simplify the analysis and design of real physical systems. Thus, to linearize a system, the magnitudes of the signals of such control system are bounded to intervals, where the system components exhibit a linear behaviour [32].

From this knowledge and to obtain a global model that emulates the dynamics of the analysed PPRV in the time and frequency domains, a register of input and output data was carried out through the described experimental setup. In doing so, an offline identification method was applied, considering the valve like a black box. Previous to system identification, the data were smoothed with a second-order low-pass Butherworth filter (fc = 20 Hz) [33] and divided into 60 and 40 % so as to attain adequate data percentages for identification and validation models.

As a first approach, two transfer functions were achieved representing the ratios between: a) the valve output pressure and input reference voltage (P_{out}/V_{ref}) and b) the valve output pressure and input airflow rate (P_{out}/Q_{in}). The first of these linear models was obtained for a constant supply absolute pressure of 7 bars with the valve output port closed (without downstream load, or valve in vacuum) utilizing as reference input signal a squared signal 1.5 Hz, 0–3 Vdc range.

In regard to the transfer function structure, it was selected from the type of experimental response observed and defined by its parameters, iteratively estimated through an algorithm based on the Levenberg-Marquard method and developed in Matlab® [33]. The best adjustment (94.64 %) of the P_{out}/V_{ref} ratio corresponds to a damped second-order linear model without delay, which agrees with previous models for industrial applications [18, 23–25]. Finally, the adopted transfer function was

$$G_{V_{ref}}(s) = \frac{1.01}{(1 + 0.041s)(1 + 0.023)}. \quad (6)$$

Besides, the P_{out}/Q_{in} ratio obtained describes the effect on valve output pressure of input flow rate disturbances generated by the PAM operation supporting a weight of 893 N [15]. As supply pressure and input reference voltage, constant values of 7 bar absolute pressure and 3 V were, respectively, selected. Then, applying a similar procedure to the previous one, the transfer function representing the P_{out}/Q_{in} ratio for the PPRV-PAM system was

$$G_{Q_{in}}(s) = \frac{-0.922(1 + 0.927s)}{(1 + 0.041s)(1 + 0.023s)(1 + 0.927s)} \quad (7)$$

corresponding to a damped third-order model with real zero and poles, which can be simplified to a second-order model due to it has a zero and a polo in the same location.

Finally, from the superposition principle [32] and in accord with the type of controller within the analysed pneumatic valve [29], the PPRV global dynamics is represented by its output pressure, generically written as sum of its specific transfer functions multiplied by the respective inputs:

$$P_{out} = \frac{K_1 * G_{V_{ref}}(s) * G_{Q_{in}}(s)}{1 + G_{V_{ref}}(s) * G_{Q_{in}}(s)} V_{ref} + \frac{K_2 * G_{Q_{in}}(s)}{1 + G_{V_{ref}}(s) * G_{Q_{in}}(s)} Q_{in} \quad (8)$$

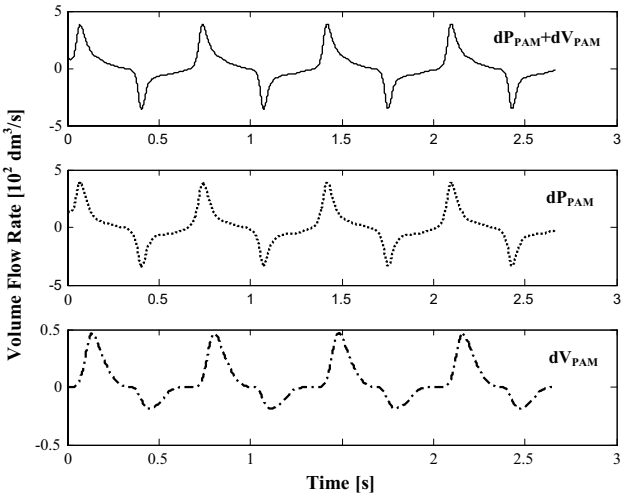

Fig. 5 Valve output flow rate for a reference input signal of 3 V, frequency 1.5 Hz

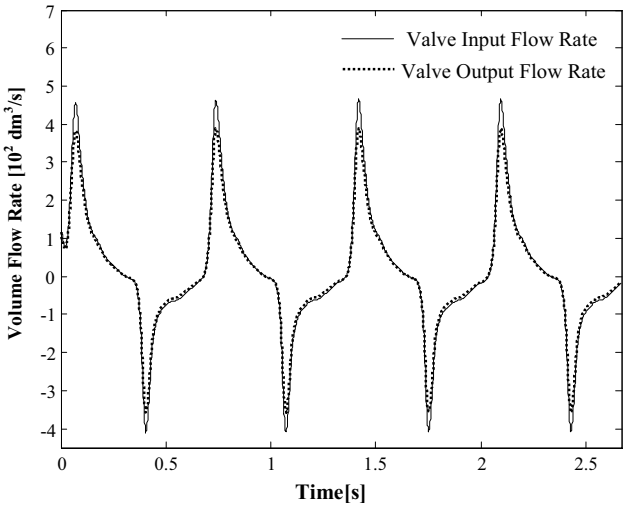

Fig. 6 Valve input and output flow rates for a reference input of 3 V, frequency 1.5 Hz

being the denominator a second-order transfer function with real poles at the left-half of the s plane.

6 Results

6.1 Airflow through the valve—pneumatic muscle actuator system

Figure 5 illustrates the results of the estimated values of valve output flow rate for the PPRV-PAM system, with reference voltages in the range 0–3 V at a frequency of 1.5 Hz. In this figure, the upper curve represents the combined

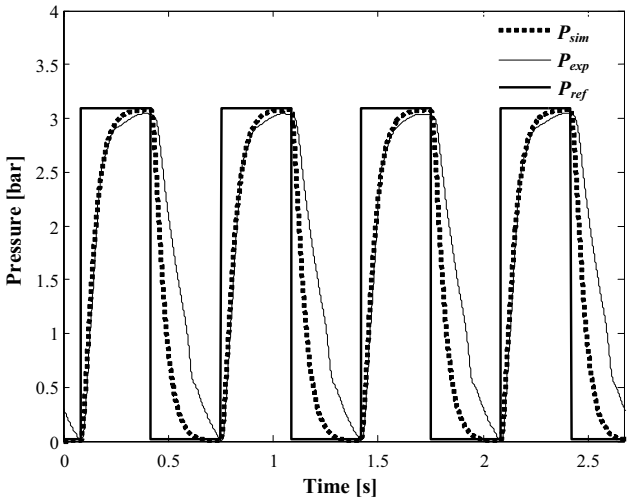

Fig. 7 Comparison between experimental (*P*exp) and simulated (P_{sim}) temporal data for the P_{out}/V_{ref} ratio of the PPRV in vacuum, squared input voltage 0–3 V, $f = 1.5$ Hz. P_{ref} reference pressure

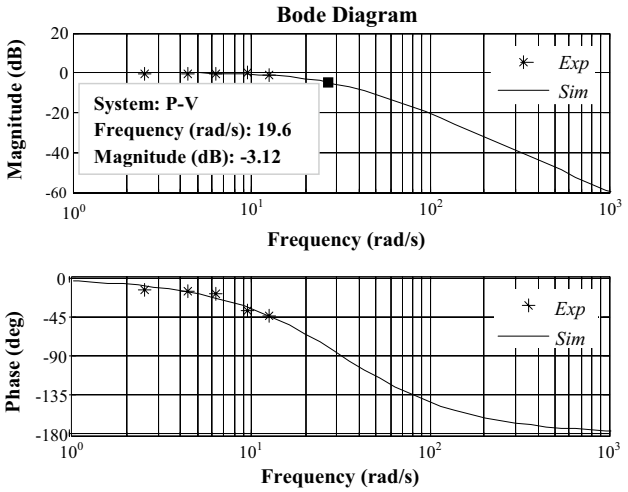

Fig. 8 Comparison between experimental and simulated frequency data for the P_{out}/V_{ref} ratio

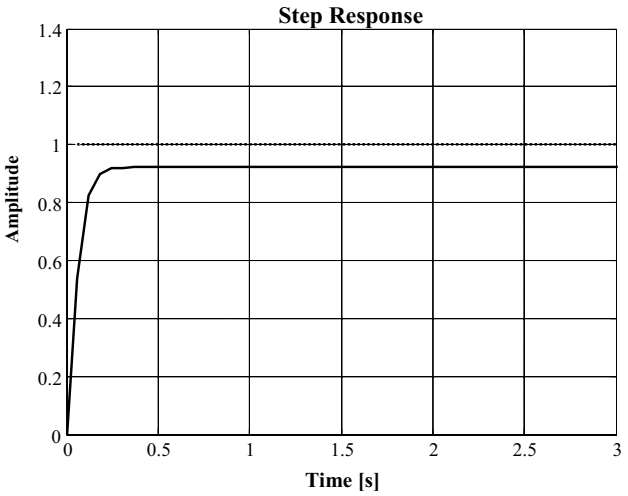

Fig. 9 Step response of the transfer function for the P_{out}/Q_{in} ratio

contribution that the PAM pressure and volume variations (named dP_{PAM} and dV_{PAM}, respectively) made to the flow rate through the valve; meanwhile, the middle and lower curves show the separate contributions of these variables on the valve flow rate.

As can be seen in Fig. 5, the contribution of dV_{PAM} is about 10 % of the total output flow rate. Similar calculations were made for a reference voltage of 5 V. Besides, the maximal values of valve input flow rate were 2.79 l/min and 4.34 l/min for reference voltage of 3 and 5 V respectively, thus indicating a concomitant raise in airflow rate through PPRV with the input reference voltage.

In addition, in Fig. 6, a comparison between the valve inlet and outlet airflow rates for the PPRV-PAM system is represented for a reference signal of 3 V. It can be seen a difference of around 20 % between the valve inlet and outlet flow rates due to the airflow rate variation within the valve, in agreement with the ideal gases state and the continuity equations [17].

6.2 Individual and global valve models

Figure 7 displays the results of the temporal validation of the model representing the P_{out}/V_{ref} ratio, evaluated for a squared reference input with peak values of 0–3 V, frequency of 1.5 Hz, and for a condition of valve closed outlet port (mean square error, MSE = 0.304). Different input signal frequencies were applied to this model in the same condition, being the MSE between simulated and experimental data equal, respectively, to 0.3183 and 0.2270 for frequencies of 1 and 0.7 Hz.

As well, Fig. 8 depicts the results of frequency validation of the PPRV P_{out}/V_{ref} ratio model in terms of Bode-diagram, with a 3.12 Hz bandwidth. However, in assessing the behaviour of this model with experimental data from the PPRV-PAM system, it showed a slower dynamics, therefore, justifying the requirement of a more precise model for describing the dynamics of this system.

In contrast, Fig. 9 exhibits the step response of the P_{out}/Q_{in} ratio model, characterising the effect on valve output pressure of the input airflow rate disturbance due to downstream load variations during PAM operation (MSE = 0.078). The static gain value is −0.922; meanwhile, the poles at the left-half of the *s* plane (common to both specific transfer functions) show a stable PPRV behaviour.

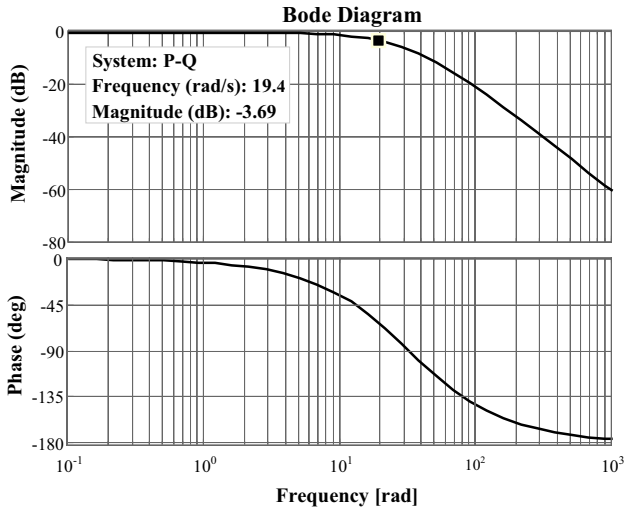

Fig. 10 Frequency response for the transfer function of the P_{out}/Q_{in} ratio

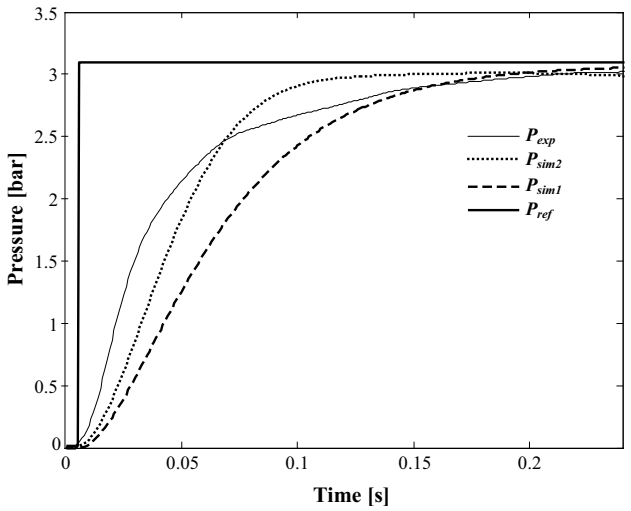

Fig. 11 Validation results for the PPRV. P_{ref} reference pressure, P_{sim1} P_{out}/V_{ref} ratio simulated response, P_{sim2} global model simulated response, P_{exp} measured valve output pressure

In addition, Fig. 10 shows the visualised Bode diagrams of the PPRV frequency response in terms of its flow rate input, where the estimated bandwidth for the P_{out}/Q_{in} ratio, evaluated with the valve output port connected to the PAM supporting a weight of 893 N, is 3.69 Hz.

Finally, Fig. 11 displays the temporal validation of the PPRV global model, achieved from the comparison of real and simulated data through a block diagram made in Matlab–Simulink®.

In Fig. 11, P_{ref} signals a valve reference output pressure of 3 bar; meanwhile, P_{exp} refers to the measured data when the valve outlet port is downstream connected to the PAM supporting a weight of 893 N. The temporal response analysis of the PPRV global model (P_{sim2}) evaluated in this condition shows a better approach (MSE = 0.0499) as regard the response of the PPRV model for the P_{out}/V_{ref} ratio (P_{sim1}) evaluated in vacuum (MSE = 0.1663), thus demonstrating that the global model provides a better estimation of PPRV dynamics at the variable downstream load condition imposed by PAM operation.

7 Conclusions and discussion

This comprehensive work was oriented to identify, model, and validate the dynamics of a PPRV not characterised until now, as is the case of the valve-type Festo® VPPM 6L-L-1-G18-0L10H-V1 [29]. We plan to use such a type of pneumatic valve for controlling the PAM operation as part of an actuation system within an active ankle–foot orthosis (AAFO) for gait rehabilitation in iSCI patients [1–4]. The final aim is to assist the ankle joint during gait training with the AAFO, which requires design a suitable actuation scheme based on a PPRV-PAM system to simultaneously attain a smooth joint movement and an efficient interaction force with the patient [5–7].

In such a sense, due to the dynamic effect on the valve output pressure (the controlled variable P_{out}, symbolized in Fig. 1) of their both inputs (the reference voltage V_{ref} and disturbances Q_{in} caused by PAM operation), the main contributions of this paper are related to: (a) the development of a detailed methodology, based on the basic principles of pneumatic systems, to estimate the valve outlet and inlet airflow rate for the PPRV-PAM system; (b) the attainment of a new PPRV global linear model in terms of its both reference voltage and airflow rate inputs for the variable load condition imposed by PAM operation; and (c) the analysis and validation of this model in the time domain.

As regard the obtained valve global model, although it does not consider the typical non-linearity of pneumatic systems, the model validation result (MSE = 0.0499) allows us to say that this model is a good approach to describe the analysed PPRV dynamics. Besides, both individual linear models (P_{out}/V_{ref} and P_{out}/Q_{in} ratios) have a similar frequency response, and thus, the 3.69 Hz bandwidth of the PPRV global model is within the human gait frequency range [19, 20].

On the other hand, to search cues to design a suitable actuation scheme based on a PPRV-PAM system within an AAFO for gait rehabilitation, we take as a starting point of our analysis the variable compliant behaviour shown by a pneumatic artificial muscle (PAM). Indeed, it is known that all pneumatic actuators show a natural compliance due to the air compressibility [17]. In addition, the PAM has another source of compliance from it varying effective area,

determined by the force dropping in relation to the contraction [13, 14]. For the type of PAM here analysed [30], such compliance C, defined as the inverse of stiffness K (N/m), can be calculated from

$$K = C^{-1} = \frac{\mathrm{d}F_{\mathrm{PAM}}}{\mathrm{d}x} = -\left(\frac{\mathrm{d}V_{\mathrm{PAM}}}{\mathrm{d}x}\right)^2 \frac{\mathrm{d}p_{\mathrm{PAM}}}{\mathrm{d}V_{\mathrm{PAM}}} - \frac{\mathrm{d}^2 V_{\mathrm{PAM}}}{\mathrm{d}x^2} p_{\mathrm{PAM}}. \tag{9}$$

In this expression, F_{PAM} symbolizes the muscle force, while the minus sign of both the right-hand side terms indicates the inverse variation between the muscle force and muscle contraction.

An analysis of (9) points out that the first term, characterising the change of pressure with PAM volume, is function not only of the air compressibility, but also of the airflow from or to this volume. As well, the second term of (9) describes the PAM stiffness at isobaric conditions, only attributed to its effective area variation. Equation (9) additionally signals that an increase of pressure determines a consequent growing stiffness and, thus, a diminishing compliance.

Furthermore, the PAM stiffness rate-of-change can be obtained from the derivative of (9) as

$$\begin{aligned}\frac{\mathrm{d}K}{\mathrm{d}t} &= \frac{\mathrm{d}C^{-1}}{\mathrm{d}t} = -\left(\frac{\mathrm{d}V_{PAM}}{\mathrm{d}x}\right)^2 \frac{\mathrm{d}x}{\mathrm{d}t}\frac{\mathrm{d}p_{PAM}}{\mathrm{d}V_{PAM}} - \frac{\mathrm{d}^2 V_{PAM}}{\mathrm{d}x^2}\frac{\mathrm{d}x}{\mathrm{d}t} p_{PAM} \\ &= -\frac{\mathrm{d}V_{PAM}}{\mathrm{d}x}\dot{p}_{PAM} - \frac{\mathrm{d}^2 V_{PAM}}{\mathrm{d}x^2}\dot{x}p_{PAM}\end{aligned} \tag{10}$$

where a rearrangement of variables was made in the right-hand side terms.

Finally, comparing (10) with (11):

$$q = \frac{V_{\mathrm{PAM}}}{\kappa RT}\dot{p}_{\mathrm{PAM}} + \frac{1}{\kappa RT}\frac{\mathrm{d}V_{\mathrm{PAM}}}{\mathrm{d}x}\dot{x}p_{\mathrm{PAM}} \tag{11}$$

The equivalence between both expressions becomes evident, which is verified from the estimated values of the PAM stiffness rate-of-change and the valve input airflow rate when the PAM is downstream connected to the valve, as shown in Fig. 12.

This enables us to obtain the following relevant conclusion: the airflow rate variation through the valve is linked to the PAM stiffness rate-of-change in direct sense and, therefore, with the PAM compliance rate-of-change in inverse sense. As well, this change is dependent both on the pressure and contraction derivatives. The potentiality of this correlation could orient us to explore in future works, how simultaneously attain a smooth joint movement and an efficient interaction force with the patient through a PPRV-PAM actuation system within an AAFO for gait rehabilitation.

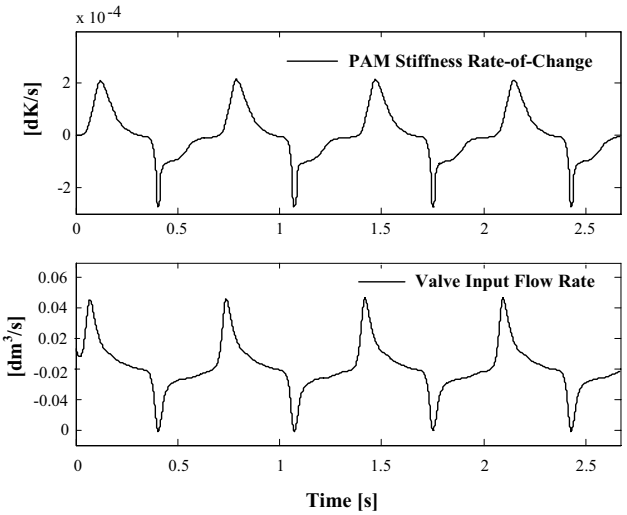

Fig. 12 Comparison between the PAM stiffness rate-of-change (*upper figure*) and the valve input flow rate (*lower figure*) for a reference input signal of 3 V, frequency 1.5 Hz

Besides, it is desirable that such PPRV-PAM actuation system be able to mimic the dynamic adjustment that the ankle joint, controlled by signals from the human central nervous system, achieves on its mechanical stiffness through a change of both the articular movement and muscle activity level during gait cycle [5–7]. Mostly, this matter takes relevance at about 60 % of gait cycle, where the ankle plantar-flexor muscles generate the main active power of the human neuromuscular system so as to ensure forefoot takeoff and propel the lower limb from gait stance to swing phase.

From these issues, we can hypothesise that an efficient PPRV-PAM actuation system as part of an AAFO for gait rehabilitation must be capable to: (a) emulate the dynamic regulation exerted by the central nervous system on the plantar-flexor muscle group during normal gait and (b) to simultaneously modify the PAM level of force and position with the objective of applying an articular power equivalent to those of plantar-flexor muscle group throughout the gait cycle.

Such PPRV-PAM system dynamics must be provided by the PPRV reference input. From a suitable control scheme regulating both the waveform and magnitude of this reference signal, it is expected that the PPRV matches the activation dynamics of the central nervous system, whereas the PAM imitates the contraction dynamics of the plantar-flexor muscles during gait cycle [36]. The input voltage waveform and intensity would affect too, the valve input flow rate waveform and intensity, thus varying the PAM stiffness rate-of-change and its inverse, the PAM compliance rate-of-change.

Note that, meanwhile, a PAM can produce only unidirectional force, moving a joint requires a setup of antagonistic muscles. A basic setup includes two PAMs (each one operated, e.g., by a PPRV to achieve an agonist/antagonist pair of PAMs) and a revolute joint around which the AAFO structure generates ankle dorsi-flexion and plantar-flexion movements in the sagittal plane [11, 12].

As example, the use of an agonist/antagonist pair of PAM's muscles to attain simultaneous control of position and stiffness similar to the human nervous system has been proposed [37]. Likewise, an adequate articular power through a selective compliance was got, achieving the same position of the AAFO ankle joint at different settings of the PAM stiffness or its inverse, the PAM compliance. For this basic setup, the ankle joint position will depend on the difference of both valve output pressures, whereas the joint stiffness of the sum of these pressures.

Based on this background, our further work is oriented in three steps: (1) to achieve an overall simulation model for the PPRV-PAM system to study the dynamic performance of the whole pneumatic system, based on the previous models about central nervous system activation dynamics and muscle contraction dynamics that take place during normal gait [38, 39]; (2) to design and validate effective control schemes for this simulation model; and (3) to implement the best solution of the proposed control schemes on the AAFO structure for gait rehabilitation in iSCI patients, which is the essential goal of the research exposed in this comprehensive work.

Finally, as a general conclusion of this work, we can say that it constitutes a reference procedure for globally characterising the PPRV dynamic behaviour for a situation, where the PAM force and position need to be precisely controlled via the valve, as it is the particular case of our intended application referred to the AAFO for gait rehabilitation in iSCI patients.

Acknowledgments The authors would like to thank Universidad Nacional de San Juan and Government of San Juan province for the financial support, as well as the staff of the Institute of Materials and Soils for their technical assistance.

Appendix

In this section, the methodology used for mapping the analysed PPRV airflow rate working space, in agreement with the standard ISO 6358 is detailed [31]. As was previously mentioned, the air flow rate through the PPRV is described by the sonic conductance C and the critical pressure ratio b, related to the expressions (1) and (2).

Although this standard details the measurement setup suitable to estimate the dependence of C and b with respect to the valve diaphragm aperture degree, the preparation of special equipment for holding the diaphragm in a constant position for each supply pressure is very expensive and work intensive. Thus, due to the C and b values that have not been informed by the valve manufacturer, in this work, we consider an alternative procedure for estimating these parameters. Such procedure is based on charging and discharging a constant volume tank through the valve evaluated at isothermal conditions [34, 35]. In agreement with the state equation of ideal gases [17], the pressure variation at the valve downstream connected to a pneumatic load can be expressed as

$$\dot{p}_{\text{out}} = \frac{\kappa RT}{V} q - p_{\text{out}} \frac{\dot{V}}{V} \tag{12}$$

where $\dot{p}_{\text{out}}$ is the valve output pressure derivative (bar/s); κ is the conversion factor; R is the gas ideal constant = 286,9 (J/Kg °K); V is the container volume (m^3); and $\dot{V}$ is the container volume derivative (m^3/s).

When this load represents a constant volume tank, the second term of (12) is null. Then, by linking (12) with (1) and (2), the derivative of pressure in the downstream tank can be attained as

$$\dot{p}_{\text{out}} = \frac{\kappa RT_{\text{out}}}{V_{\text{out}}} Cp_{\text{in}} \sqrt{\frac{T_{\text{in}}}{T_{\text{out}}}} \sqrt{1 - \left(\frac{\frac{p_{\text{out}}}{p_{\text{in}}} - b}{1 - b} \right)^2} \quad \text{for } \frac{p_{\text{out}}}{p_{\text{in}}} \rangle b \quad \text{subsonic flow} \tag{13}$$

$$\dot{p}_{\text{out}} = \frac{\kappa RT_{\text{out}}}{V_{\text{out}}} Cp_{\text{in}} \sqrt{\frac{T_{\text{in}}}{T_{\text{out}}}} \quad \text{for } \frac{p_{\text{out}}}{p_{\text{in}}} \leq \text{b} \quad \text{chocked flow.} \tag{14}$$

The values of C and b were estimated utilizing these expressions based on the valve inlet and outlet absolute pressures registered during charging a 0.04 m^3 volume tank connected downstream to the valve through the experimental test bench described in detail in Sect. 3. Previous to estimation, an adequate filtering was applied for smoothing the measured data [33].

The first parameter was obtained from (13) and the second one, as the point where the derivative of the valve output pressure signal changes. Of note is that b value expresses the divide of the valve downstream and upstream absolute pressure for which the flow rate through it becomes choked [17, 34, 35]. Besides, the effect of the flow-rate disturbance on PPRV outlet absolute pressure was modelled according to (1) and (2) and using the C and b values previously estimated.

In contrast, for estimating C and b parameters during tank discharging through PPRV, a different methodology

Table 1 Values of b and C estimated during tank charging through PPRV

Upstream pressure (bar)	Critical pressure ratio b (−)	Sonic conductance C [m^3/(s*bar)]
1.946	0.6624	1.6668e−04
2.954	0.5972	2.1299e−04
3.964	0.5674	6.4101e−04
4.983	0.5541	7.8871e−04
5.991	0.5308	7.7140e−04
6.943	0.5328	7.0564e−04

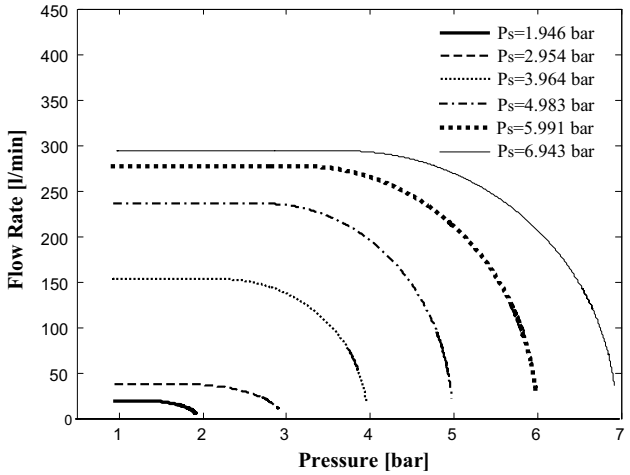

Fig. 13 Modelled PPRV flow-rate curves during charge of a constant volume tank

Table 2 Values of b and C estimated from tank discharging through PPRV

Max tank pressure (bar)	Critical pressure ratio b (−)	Sonic conductance C [m^3/(s*bar)]
1.8964	0.7464	0.0002
2.7350	0.6709	0.0003
3.9706	0.6177	0.0007
4.9714	0.5940	0.0008
5.9744	0.5782	0.0009
6.8439	0.5683	0.0007

was used, based on the *fminsearch* function for searching these parameters through an algorithm in Matlab®. The achieved C and b values were then replaced in the standard ISO 6358 expressions [31], so as to graphically obtain the output flow rate in the function of the tank pressure.

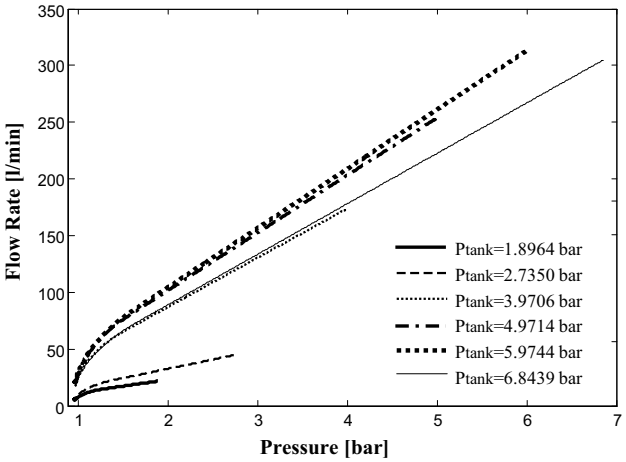

Fig. 14 Modelled PPRV flow-rate curves during a constant volume tank discharge

As part of the obtained results, Table 1 displays the values of C and b corresponding to the charge of a constant volume tank, estimated according to the standard ISO 6358 for different valve upstream absolute pressure values (1–7 bars).

In addition, Fig. 13 shows the curves of the flow rate through the valve in the same tank charging situations. In this figure, it can be observed that the flow rate through the valve is constant until the ratio of downstream and upstream pressures is larger than the critical pressure ratio b. In addition, it is shown that the increase of absolute supply pressures determines a consequent flow-rate rise. Finally, it is appreciated that the curves corresponding to the lower supply pressures display a not null flow-rate condition. This behaviour is due to the fact that the data acquisition time was minor than the time for which the valve output pressure equals the supply pressure.

Besides, Table 2 and Fig. 14 present, respectively, the estimated values of C and b and the flow rate through the valve curves during tank discharging, for absolute supply pressures among 1.9–6.8 bars.

The shape of these curves agrees with those provide at manufacture's datasheets about the flow rate from the valve output port to valve exhaust port [29]. In particular, these curves are similar for tank pressures higher than 3 bars. Besides, the C and b parameters have the same values for the different analysed supply pressures. Thus, due to their independence of the valve output pressure, the condition of tank discharging through the PPRV is described from a single pair of C and b values.

Although for obtaining a more precise model of the flow rate through the PPRV, it is still required to determine the C and b parameters as a function of valve diaphragm position;

the procedure here considered helps to identify the flow rate in the whole range of movement of the diaphragm. In future works, we plan to estimate such parameters in a function of the valve diaphragm position.

References

1. Dollar A, Herr H (2008) Lower extremity exoskeletons and active orthoses: challenges and state-of-the-art. IEEE T Robotic Autom 24:144–158
2. Veltink PH, Koopman HF, van der Helm FC (2001) Biomechatronics-assisting the impaired motor system. Arch Physiol Biochem 109:1–9
3. Colombo G, Wirz M, Dietz V (2001) Driven gait orthosis for improvement of locomotor training in paraplegic patients. Spinal Cord 39:252–255
4. Harkema S, Dobkin B, Edgerton V (2000) Pattern generators in locomotion: implications for recovery of walking after spinal cord injury. Top Spinal Cord Inj Rehabil 6:82–96
5. Winter D (2009) Biomechanics and motor control of human movement. Ed. Wiley., New Jersey
6. Giddings VL, Beaupre GS, Whalen RT, Carter DR (2000) Calcaneal loading during walking and running. Med Sci Sports Exerc 32:627–634
7. Kim S, Park S (2011) Leg stiffness increases with speed to modulate gait frequency and propulsion energy. J Biomech 44:1253–1258
8. Beyl P, Naudet J, Van Ham R, Lefeber D (2007) Mechanical design of an active knee orthosis for gait rehabilitation. In: Proceedings of the IEEE 10th International Conference on Rehabilitation Robotics, Noordwijk, Netherland, pp.100–105
9. Blaya J, Herr H (2004) Adaptive control of a variable-impedance ankle-foot orthosis to assist drop foot gait. IEEE Trans Neural Syst Rehabil Eng 12:24–31
10. Naito H et al (2009) An ankle–foot orthosis with a variable-resistance ankle joint using a magnetorheological-fluid rotary damper. J Biomed Eng 4:182–191
11. Ferris DP, Sawicki GS, Domingo A (2005) Powered lower limb orthoses for gait rehabilitation. Top Spinal Cord Inj Rehabil 11:34–49
12. Ferris DP, Gordon KE, Sawicki GS, Peethambaran A (2006) An improved powered ankle foot orthosis using proportional myoelectric control. Gait Posture 23:425–428
13. Daerden, F., 1999, "Conception and realization of pleated pneumatic artificial muscles and their use as compliant actuation elements", Ph.D. Thesis, Vrije Universiteit Brussel, Belgum
14. Ali H, Noor S, Bashi SM, Marhaban MH (2008) A review of pneumatic actuators: modelling and control. Australian J Basic Appl Sci 3:440–454
15. Lescano C, Herrera C, Mirabal Z, Rodrigo R, Rodrigo S (2013) Characterization of a pneumatic artificial muscle for its application in an active ankle-foot orthosis. J Phys Conf Ser 477(012040):1–10
16. Hosovsky A, Havran M (2012) Dynamic modelling of one degree of freedom pneumatic muscle-based on actuator for industrial applications. Tehnički Vjesnik 19:673–781
17. Beater P (2007) Pneumatic drives. System design, modelling and control. Ed. Springer, Berlin, Germany
18. Sorli M, Figliolini G, Pastorelli S (2004) Dynamic model and experimental investigation of a pneumatic proportional pressure valve. IEEE/ASME T Mech 9:78–86
19. Nilsson J, Thorstensson A (1987) Adaptability in frequency and amplitude of leg movements during human locomotion at different speeds. Acta Physiol Scand 129:107–114
20. Pépin A, Ladouceur M, Barbeau H (2003) Treadmill walking in incomplete spinal-cord-injured subjects: 2. Factors limiting the maximal speed. Spinal Cord 41:271–279
21. Ljung L (1999) System identification. Theory for the user. Ed. Prentice Hall PTR, New Jersey
22. Narendra KS, Parthasarathy K (1990) Identification and control of dynamical systems using neural networks. IEEE Trans Neural Netw 1:4–27
23. Sorli M, Figliolini G, Pastorelli S (2001) Dynamic model of a proportional pressure valve. In: Proceedings of the IEEE/ASME International Conference on Advanced Intelligent Mechatronics, Como, Italy, pp. 630–635
24. Sorli M, Gastaldi L, Quaglia G (1997) CAEPneum: a simulation tool on pneumatic elements and systems developed in MATLAB. In: Proceedings of the Fifth Scandinavian International Conference on Fluid Power, Linköping, Sweden, pp. 319–334
25. Sorli M, Figliolini G, Almondo A (2010) Mechatronic model and experimental validation of a pneumatic servo-solenoid valve. J Dyn Syst T ASME 132:054503–054513
26. Zorlu A, Ozsoy C, Kuzucu A (2003) Experimental modelling of a pneumatic system. In: Proceedings of the IEEE Conference on Emerging Technologies and Factory Automation, Lisbon, Portugal, pp. 453–461
27. Sorli M, Vigliani A (1998) Design analysis of a pneumatic force control servosystem with pressure proportional valve. J Robot Mechatron 10:370–376
28. Carneiro JF, Gomes de Almeida F, (2006) Modeling pneumatic servovalves using neural networks. In: Proceedings of the IEEE International Conference on Computer Aided Control Systems Design, Munich, Germany, pp. 790–795
29. Festo (2008) Válvulas proporcionales reguladoras: VPPM, VPPE, MPPE, MPPES, MPYE y VPPM-MPA. Festo. https://www.festo.com/net/SupportPortal/Files/26931/, Accessed 10 Jan 2015
30. Festo (2008) Fluidic Muscle DMSP/MAS, Festo: https://www.festo.com/rep/en_corp/assets/pdf/info_501/, Accessed 10 Jan 2015
31. ISO 6358 (1989) Pneumatic fluid power. Components using compressible fluids. Determination of flow-rate characteristics. International Organization for Standardization, Geneva
32. Ogata K (1997) Modern Control Engineering, Ed. Prentice Hall, New Yersey, United States of America
33. Elliot DF (1987) Handbook of Digital Signal Processing. Engineering Applications. Ed. Academic Press
34. Varga Z, Keski-Honkola P (2011) Determination of flow rate characteristics for pneumatic valves. In: Proceedings of the Experimental Fluid Mechanics Conference, Jičín, Czech Republic
35. Varga Z, Keski-Honkola P (2012) Mathematical model of pneumatic proportional valve. J Appl Sci Thermodyn Fluid Mech 1:1–6
36. Hatze H (1984) Quantitative analysis, synthesis and optimization of human motion. Hum Movement Sci 3:5–25
37. Tonietti G, Bicchi A (2002) Adaptive simultaneous position and stiffness control for a soft robot arm. In: Proceedings of the IEEE/RSJ International Conference on Intelligent Robots and Systems, Lausanne, Switzerland, pp. 1992–1997
38. Rodrigo SE, García I, Franco M et al (2010) Energy expenditure during human gait. I–An optimized model. In: Proceedings of the 32nd Annual International Conference of the IEEE-EMBS, Vol.2, Buenos Aires, Argentina, pp. 4254–4257
39. Rodrigo SE, García I, Franco M et al (2010) Energy expenditure during human gait. II–Rol of muscle groups. In: Proceedings of the 32nd Annual International Conference of the IEEE-EMBS, Vol.2, Buenos Aires, Argentina, pp. 4258–4261